Molecular BioSystems

RSC Publishing

PAPER

View Article Online
View Journal | View Issue

Cite this: *Mol. BioSyst.*, 2013, **9**, 258

Minimum set of mutations needed to optimize cyan fluorescent proteins for live cell imaging†

Marie Erard,[a] Asma Fredj,[a] Hélène Pasquier,*[a] Dahdjim-Benoît Beltolngar,[a] Yasmina Bousmah,[a] Valérie Derrien,[a] Pierre Vincent[b] and Fabienne Merola*[a]

Received 29th July 2012,
Accepted 10th November 2012

DOI: 10.1039/c2mb25303h

www.rsc.org/molecularbiosystems

Cyan fluorescent proteins (CFPs) are widely used as FRET donors in genetically encoded biosensors for live cell imaging. Recently, cyan variants with greatly improved fluorescence quantum yields have been developed by large scale random mutagenesis. We show that the introduction of only two mutations, T65S and H148G, is able to confer equivalent performances on the popular form ECFP, leading to Aquamarine (QY = 0.89, τ_f = 4.12 ns). Besides an impressive pH stability (p$K_{1/2}$ = 3.3), Aquamarine shows a very low general sensitivity to its environment, and undetectable photoswitching reactions. Aquamarine gives efficient and bright expression in different mammalian cell systems, with a long and single exponential intracellular fluorescence lifetime mostly insensitive to the fusion or the subcellular location of the protein. Aquamarine was also able to advantageously replace the CFP donor in the FRET biosensor AKAR for ratiometric measurements of protein kinase A activity. The performances of Aquamarine show that only two rounds of straightforward single point mutagenesis can be a quick and efficient way to optimize the donor properties in FRET-based biosensors.

Introduction

Biochemical imaging techniques based on Förster resonant energy transfer (FRET) and green fluorescent proteins (GFPs) are intensively used in biological, pharmacological and clinical research, to monitor specific chemical activities and molecular interactions inside living cells.[1–3] These techniques make use of chimeric genetic constructs that most often incorporate a cyan (CFP) and a yellow (YFP) variant of *Aequorea victoria* GFP (*Av*GFP) as the donor–acceptor FRET pair. However, the two most popular cyan forms, ECFP and Cerulean (ECFP-S72A-Y145A-H148D) suffer from low brightness, complex fluorescence emission decays, weak photostability and strong environmental sensitivities, which are major limiting factors in FRET imaging experiments.[4–7] Recently, greatly improved CFP variants, with fluorescence quantum yields close to unity and near-single exponential emission decays, were developed: mTurquoise[8] (ECFP-T65S-S72A-H148D-S175G-A206K, QY = 0.84), mCerulean3[9] (Cerulean-T65S-S147H-D148G-K166G-I167L-R168N-H169C-A206K, QY = 0.87) and mTurquoise2[10] (mTurquoise-I146F, QY = 0.93). As these variants were obtained through a mix of site-directed mutagenesis and medium to large scale random mutagenesis, they carry many mutations away from ECFP, whose role in the final performances remains unclear. Determining a small set of critical mutations able to confer equivalent properties to the ECFP protein would bring worthwhile lessons on its structure–photophysics relationships, would set a more robust basis for the engineering of CFPs with new functions, and would facilitate the improvement of numerous existing genetic constructs.

The newly improved CFP variants share only four common mutated positions at Thr65, Ser72, His148 and Ala206 of ECFP. The mutation A206K targets the dimerization interface of *Av*GFP and favors a monomeric state of the protein.[11,12] Due to its external location, this mutation has undetectable incidence on the fluorescence properties of ECFP.[13] The S72A mutation was introduced to improve the maturation speed of *Av*GFP variants[14] and has little impact as well on their intrinsic fluorescence properties.[15–17] In contrast, the side chains of residues 148 and 65 are located very close to the chromophore, and have a prominent influence on its photophysics.[7,18–21] We have shown recently that the T65S mutation markedly and simultaneously increases the brightness, photostability and pH insensitivity of ECFP and Cerulean, while it is associated with increased fluorescence quantum yields in many other *Av*GFP variants.[22] From the comparison of various crystallographic structures, we hypothesized that a serine in position 65 favors a native protein conformation associated with a more

[a] *CNRS, Univ Paris-Sud, Laboratoire de Chimie Physique, Orsay, France. E-mail: helene.pasquier@u-psud.fr, fabienne.merola@u-psud.fr*
[b] *CNRS, UPMC, UMR 7102 Neurobiology of Adaptative Processes, Paris, France*

† Electronic supplementary information (ESI) available. See DOI: 10.1039/c2mb25303h

rigid chromophore environment. This choice actually restores the natural aminoacid present in *Av*GFP, and was re-selected in CFP after an exhaustive random screening of this single position.[8] The most advisable mutation to be introduced in ECFP is thus certainly T65S.

Although Cerulean-T65S achieves performances very similar to mTurquoise, this is not the case of ECFP-T65S, which still requires further engineering.[22] In all best CFP variants, the T65S mutation appears well complemented by some substitution at position 148. Targeting mutations on His148 was originally motivated by the speculation that the slow and large amplitude movements of this residue, as revealed by NMR and X-ray crystallography,[23,24] were likely responsible for the multiple, weakly fluorescent subpopulations of ECFP. Indeed, introducing the H148D mutation in ECFP, which led to Cerulean,[19] improved significantly its fluorescence quantum yield. However, the H148D mutation alone does not substantially diminish the number of fluorescent subpopulations,[6] while Cerulean has a decreased photostability as compared to ECFP.[5,22] After screening for the best single substitution at position 148, we show here that the two mutations H148G and T65S are sufficient to warrant fluorescence properties comparable to the best published CFP variants (QY = 0.89 and near-single exponential emission decay). We also show that these improvements come together with a strongly decreased environmental sensitivity and enhanced photostability. Finally, we demonstrate that this new, minimally engineered ECFP variant, entitled Aquamarine, is fully adequate for high performance, quantitative live cell imaging experiments.

Results and discussion

We screened first different aminoacid replacements at position 148 of ECFP, looking for net increases in both fluorescence quantum yield (monitored through the average fluorescence lifetime, τ_f) and pH stability (monitored through the p$K_{1/2}$ of fluorescence loss at acid pHs). The best mutations were then combined with the T65S mutation, as well as with the S72A and A206K mutations. The obtained mutants all displayed very similar, double-hump spectra, characteristic of fluorescent proteins carrying an indole-based chromophore (Fig. 1A), but were associated with quite varied τ_f and p$K_{1/2}$ (Table 1). Overall, the latter two parameters displayed a striking general correlation (Fig. S1, ESI†), suggesting that common structural or dynamic features determine both the intensity of ECFP fluorescence and its pH sensitivity.

In comparison with the already described aspartate substitution at position 148,[6,19] we tried introducing either small, non-protonable residues (serine, glycine, alanine, asparagine), or residues with larger sizes (glutamic acid, arginine), that would not induce pH-dependent responses and/or would not be prone

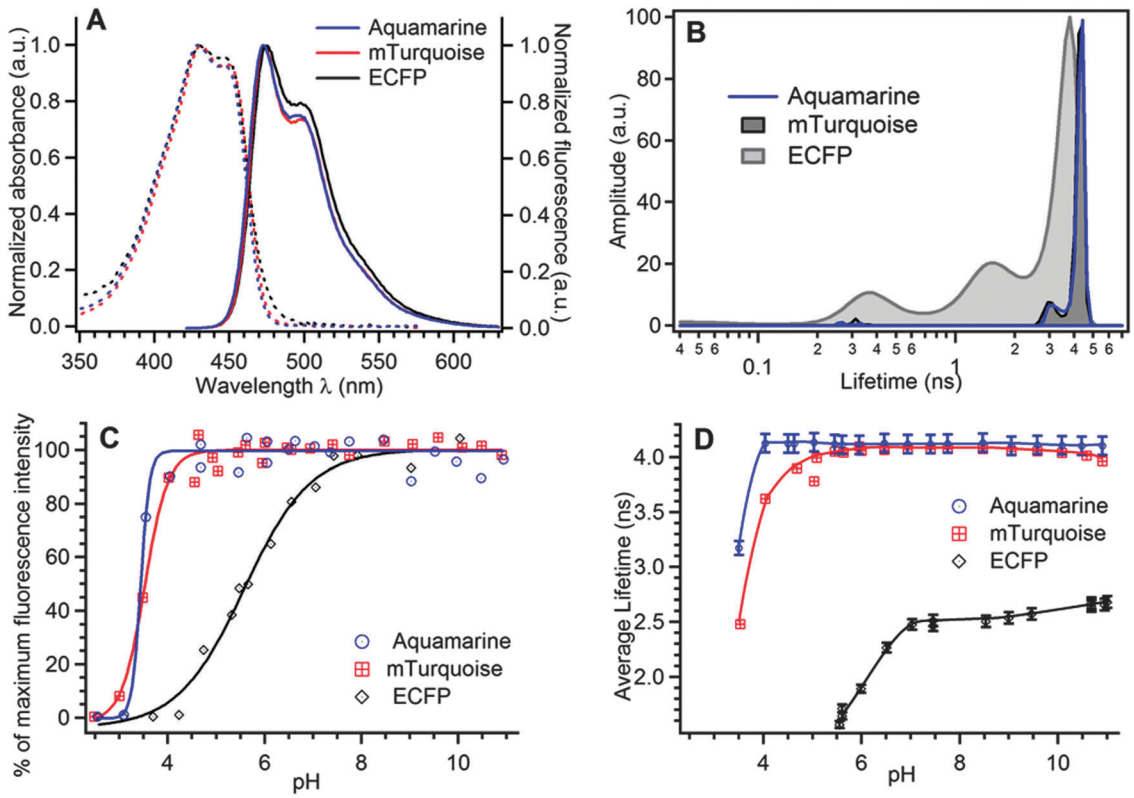

Fig. 1 Photophysical properties of purified Aquamarine. (A) Absorption (dashed lines) and emission (solid lines) spectra normalized to maximum of the chromophore band. Emission spectra were recorded with excitation at 420 nm. (B) Fluorescence lifetime distributions at neutral pH obtained from MEM analysis of the fluorescence decay curves. (C) pH dependence of the fluorescence intensity excited at 420 nm and detected at 474 nm ($\Delta\lambda$ = 6 nm). Solid lines correspond to the best fits to a sigmoidal analytical model. Experimental data were normalized to 100% maximum of their analytical fits. (D) pH dependence of the average fluorescence lifetime determined from integration of the lifetime distributions. Solid lines are for eye guidance only.

Table 1 Comparison of various purified mutants of ECFP

Mutant	τ_f (ns) ± 0.05 ns	p$K_{1/2}$ ± 0.1	Mutant	τ_f (ns) ± 0.05 ns	p$K_{1/2}$ ± 0.1
ECFP	2.50	5.6	mTurquoise	4.06	3.4
ECFP (148D)	3.30	5.5	ECFP (65S, 148D)	4.02	4.0
ECFP (148E)	3.15	5.1	ECFP (65S, 148E)	3.86	4.1
ECFP (148S)	3.17	4.5	ECFP (65S, 148S)	3.86	3.6
ECFP (148G)	3.37	4.9	ECFP (65S, 148G) *Aquamarine*	4.12	3.3
ECFP (148A)	3.15	4.5	Cerulean	3.06	5.2
ECFP (148N)	2.93	5.7	Cerulean (148G)	3.13	4.4
ECFP (148R)	2.04	5.7	Cerulean (65S)	3.95	3.6
ECFP (65S)	3.30	4.5	ECFP (65S, 148D, 72A, 206K)	4.05	3.9
ECFP (65S, 72A, 206K)	3.38	4.8	ECFP (65S, 148G, 72A, 206K) *Aquamarine*-72A-206K	4.06	3.1

to adopt multiple conformations. As a general rule, substitutions by short, non-protonable residues (S,G,A) brought the most significant improvements (Table 1). Then, the combination of these single point mutations with the T65S mutation led to further ameliorations in both τ_f and p$K_{1/2}$. Among all variants tested, a short and apolar glycine at position 148, combined with the T65S mutation, leads to the best performances, with τ_f = 4.12 ns, and p$K_{1/2}$ = 3.3 (Table 1). We decided to name this new variant, carrying a minimal set of mutations away from ECFP, Aquamarine. It is interesting to note that the H148G mutation was also identified as a beneficial mutation during the development of both mTurquoise[8] and mCerulean3,[9] after random screenings or site-directed saturation mutagenesis of the (148, 224) and (147, 148) pairs of aminoacids respectively. Consistently also, exchanging the aspartate 148 of Cerulean for a glycine improves both its average lifetime and its p$K_{1/2}$ (Table 1). Introducing the two mutations S72A and A206K into Aquamarine and other CFPs brings only marginal changes to their fluorescence properties (Table 1), except for a further extension of the stability of Aquamarine at very acid pHs (Fig. S2, ESI†). Taken together, our results indicate that the double substitution (T65S, H148G) in ECFP is a necessary and sufficient condition to reach photophysical performances at least equivalent to those of mTurquoise.

We then characterized in more detail the fluorescence properties of Aquamarine in comparison to ECFP and mTurquoise. In keeping with its long fluorescence lifetime, the quantum yield of Aquamarine is remarkably high (QY = 0.89) and comparable to those of the best CFP mutants recently published.[10] The fluorescence emission decay of Aquamarine, measured at high temporal and statistical accuracy, follows a near-single exponential, dominated by 89% of a long lifetime component at 4.29 ns ± 0.09 ns (Fig. 1B). As all CFPs, Aquamarine undergoes a complete loss in fluorescence intensity at very acidic pHs (Fig. 1C), accompanied by a blue shift and a loss of the double-hump structure of its spectra (Fig. S3, ESI†). Similarly to mTurquoise and Cerulean-T65S,[22] and in contrast to ECFP (Fig. 1C), this acid transition is very steep and highly cooperative, with the first acid-induced spectral perturbations appearing only for pHs lower than 3.6 (Fig. S3, ESI†). Interestingly, the average fluorescence lifetime of Aquamarine also remains stable over a very large domain of pHs, from pH 3.5 to pH 11, while for mTurquoise, this pH-stability covers a narrower domain ranging from pH 5 to pH 11 (Fig. 1D).

As discussed in ref. 22, a high quantum yield and a marked simplification in the fluorescence emission kinetics likely reflect an increased local rigidity and hindering of the CFP chromophore torsions, which, as a general rule, might contribute also to decrease its environmental sensitivity. For example, the fluorescence intensity and lifetime of ECFP display a pronounced and parallel dependence on temperature,[6] which is strongly reduced in Aquamarine and mTurquoise: while the average fluorescence lifetime of cytosolic ECFP decreases by 21% between 20 °C and 37 °C, those of Aquamarine and mTurquoise are only reduced by 8%. It is known also that ECFP displays a peculiar sensitivity to millimolar concentrations of ATP,[7] which is absent in Aquamarine and mTurquoise, as well as in Cerulean (Fig. S4, ESI†).

Therefore, Aquamarine, obtained after only two mutations away from ECFP, achieves photophysical performances equivalent to the best cyan variants. The possibility to use Aquamarine for live cell imaging also depends on its ability to fold and mature efficiently, in a delay compatible with cell culture growth. Exchanging the wild-type serine 65 for a threonine in *Av*GFP markedly accelerated the growth of fluorescence in *E. coli* cultures.[18] Although Aquamarine carries the ECFP mutations F64L, M153T and V163A, meant also to improve folding efficiency,[14,16] the T65S mutation combined with lack of the S72A mutation might be disadvantageous as compared to other improved variants. We observed that the rise of Aquamarine fluorescence in *E. coli* cultures is delayed by about 2 hours as compared to mTurquoise, and by 5 hours as compared to ECFP (Fig. S5, ESI†). The value of the molar extinction coefficient of purified Aquamarine (26 000 ± 3000 L mol^{-1} cm^{-1} at 430 nm) shows that the final level of *in vitro* chromophore maturation is comparable to other CFP variants.[10,22] We also obtain equivalent fluorescence recovery times at 37 °C for Aquamarine (970 ± 400 s) and mTurquoise (1140 ± 240 s) after extensive *in vitro* denaturation and reduction. These times are however about twice that of ECFP (500 ± 100 s), which is likely the counterpart for an increased rigidity.

The expression of fluorescent proteins in bacteria, or their folding properties *in vitro*, are rather poor predictors of their behaviour in eukaryotic systems.[16,25,26] A more decisive criterion is thus the effective brightness achieved by Aquamarine in mammalian cell cultures. The fluorescence intensity was

measured by flow cytometry 24 hours after transfection of MDCK cells by equal amounts of plasmids encoding cytosolic ECFP, mTurquoise or Aquamarine. The percentage of fluorescent cells was comparable for the three variants (10 ± 2%), with a good reproducibility of the transfections. On average at 20 °C, cells expressing mTurquoise and Aquamarine were respectively 1.6-fold and 1.75-fold more fluorescent than those expressing ECFP. Owing to their different sensitivity to temperature (see above), these ratio should rise, respectively, to 1.9 and 2 at 37 °C, in agreement with reported data on mTurquoise.[8] Therefore, Aquamarine expresses and matures fairly efficiently, and comparably to mTurquoise, in mammalian cells at 24 hours after transfection. However, a prior evaluation of Aquamarine might be recommended in cases requiring a very rapid onset of the fluorescence.

We then used Aquamarine for various cell imaging experiments in model cell lines. Aquamarine was efficiently expressed in MDCK cells as a cytosolic protein, fused to the C-terminus of connexin 43[27] or targeted to the plasma membrane by a N-terminus MyrPalm anchor[28] (Fig. 2A). Aquamarine was also successfully incorporated in a FRET biosensor expressed in BHK cells (see below). In all cases, most of the Aquamarine fluorescence was observed at the expected location, without any traces of aggregation in intracellular organelles. All together, these results demonstrate that the expression, folding and maturation of Aquamarine are fully adequate for live cell applications. We then evaluated the improvements brought by Aquamarine in quantitative fluorescence imaging.

The fluorescence intensities of Aquamarine transfected cells allowed the routine collection of high contrast images by laser scanning TCSPC FLIM in less than 30 s (Fig. 2B), from which accurate fluorescence decays could be built over small ROIs (Fig. 2C and D). With our FLIM set-up, we obtain an average fluorescence lifetime for cytosolic ECFP of 2.55 ± 0.06 ns at 20 °C, in full agreement with the literature.[4,29] In all live cell expression systems, the fluorescence decays of Aquamarine were much less complex than for ECFP. Cytosolic Aquamarine and mTurquoise have similar, near-single exponential fluorescence decays, with respective average lifetimes of 3.95 ± 0.03 ns and 3.90 ± 0.06 ns, the latter being in good agreement with literature data.[8,9,30] Myristoyl and palmitoyl chains target the fluorescent protein mainly to the lipid rafts of the plasma membrane.[11,28] After introduction of the two mutations of Aquamarine, T65S and H148G, the fluorescent construct displayed a similar membrane location (Fig. 2A), but a much less complex fluorescence decay (Fig. 2D): while the average lifetime of MyrPalm–CFP was 1.60 ± 0.10 ns, that of MyrPalm–Aquamarine was 3.73 ± 0.06 ns. The average fluorescence lifetime of membrane-targeted MyrPalm–Aquamarine was therefore only 6% shorter than cytosolic Aquamarine, a small decrease that may reflect a higher local refractive index in the vicinity of the membrane.[31] Similarly, despite a highly confined location at intercellular gap junctions (Fig. 2A), the average fluorescence lifetime of Cx43–Aquamarine remains very high (3.90 ± 0.10 ns), with a fluorescence decay close to a single exponential (Fig. 2D).

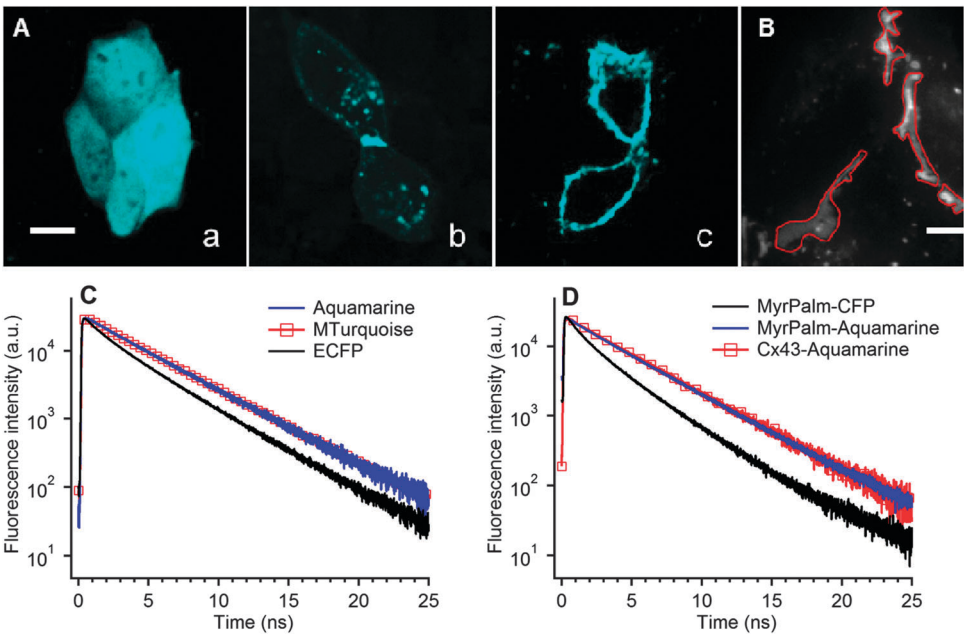

Fig. 2 Fluorescence imaging and TCSPC fluorescence decays of Aquamarine in living MDCK cells. (A) Confocal fluorescence microscopy images of Aquamarine expressed at different locations: (a) cytosolic expression, (b) Cx43 fusion and (c) MyrPalm membrane anchor. (B). Intensity image built from time-resolved laser scanning TCSPC microscopy. Fluorescence photons collected from the appropriate ROIs (in red) were used to calculate the corresponding fluorescence decays. In this example, the fluorescence from Cx43–Aquamarine in selected gap junction areas was collected. Scale bars 10 μm. Comparison of TCSPC fluorescence decays of (C) cytosolic ECFP, mTurquoise and Aquamarine and (D) MyrPalm–CFP, MyrPalm–Aquamarine and Cx43–Aquamarine. Decays were adjusted to the same maximum intensity for comparison.

The extended acid stability of Aquamarine fluorescence may be particularly advantageous when the local pH varies, in specialized cell compartments or according to specific signaling events.[21,32] To mimic these conditions, we varied the intracellular pH of MDCK cells by use of the nigericin ionophore in the presence of an external acid buffer. While the pH was changed from neutral to pH 5.9, the average fluorescence lifetime of cytosolic ECFP decreased by 17 ± 2%, while the Aquamarine lifetime remained constant (Fig. 3A). ECFP and Cerulean are also prone to reversible photoswitching reactions, characterized by a pronounced transient loss in fluorescence intensity upon sudden illumination, and fluorescence recovery times in the dark of the order of several minutes.[5,22,33] These photoreactions can contribute significantly to the variability of FRET signals (ref. 9, and see below). We have shown previously that CFP photoswitching reactions are strongly reduced by the T65S mutation, probably due to hindering of the chromophore *cis–trans* photoisomerization:[22] similarly to mTurquoise, the photoswitching of cytosolic Aquamarine is nearly undetectable (Fig. 3B). We also checked the long term photostability of Aquamarine under prolonged wide-field illumination of MDCK cells expressing cytosolic ECFP, mTurquoise and Aquamarine. Under similar 30 min illumination with 0.2 W cm^{-2} irradiance, the decay time for irreversible bleaching of mTurquoise at 20 °C was 1480 ± 180 s, that of Aquamarine was 900 ± 110 s, and that of ECFP 730 ± 90 s. Therefore, although Aquamarine does not fully equate the already reported remarkable photostability of mTurquoise,[10,22] it is significantly improved as compared to ECFP.

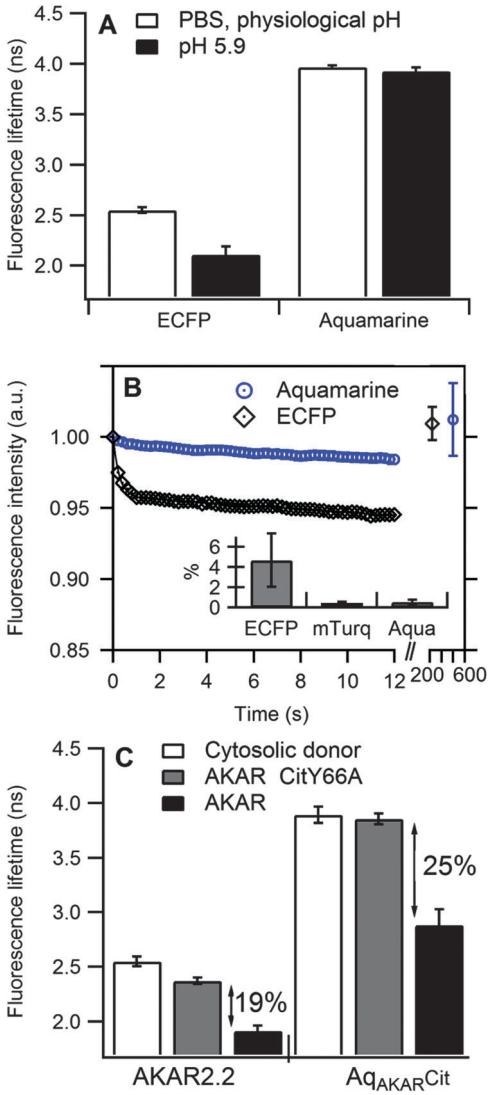

Fig. 3 Fluorescence properties of Aquamarine in live cells. (A) Variation of the cytosolic fluorescence lifetime of Aquamarine and ECFP with pH. (B) Reversible photoswitching of cytosolic CFPs. The decay of mTurquoise was similar to Aquamarine's decay and thus not represented for clarity. Continuous lines are best fits to the model $F_{norm} = y0 + y1t + y2\ \exp(-t/\tau)$, where $y0$ stands for constant background and $y1$ describes the slow simultaneous irreversible photobleaching. The amplitude $y2$ of reversible photobleaching is plotted in the inset. (C) Fluorescence lifetimes of CFP (right) and Aquamarine (left) as donors in the resting states of AKAR2.2 and ^{Aq}AKAR^{Cit} respectively (dark), compared to the lifetime of the corresponding cytosolic protein (white), and after the Y66A mutation in the Citrine acceptor (grey).

It has been shown earlier that the fluorescence lifetime of ECFP changes during irreversible photobleaching.[4] We found that ECFP, mTurquoise and Aquamarine all exhibit a similar decrease of their average lifetime upon photobleaching (Fig. S6, ESI†). In addition, the proportionality relationship between lifetime and quantum yield is not maintained, as the fluorescence intensity drops by 90%, while the fluorescence lifetime decreases by only 30%, consistently with a previous report on mTurquoise.[30] This shows that the photobleaching of CFPs is the result of two phenomena: formation of a dark population that contributes to the fast decrease of fluorescence intensity, and irreversible modifications of the remaining fluorescent population, leading to changes in fluorescence lifetimes. As a consequence, any significant bleaching should be carefully avoided during FLIM acquisitions.

We then checked the ability of Aquamarine to replace ECFP in FRET experiments together with its usual yellow acceptors EYFP and Citrine. When Aquamarine is introduced into a simple, non-responsive tandem construct connected to EYFP through a 27 aminoacid linker, its fluorescence lifetime decreases to 2.52 ± 0.06 ns, corresponding to an average FRET efficiency of 36 ± 2% ($\langle E_{app} \rangle = 1 - \tau_{Tandem}/\tau_{Aq}$), which is slightly higher than the apparent 33% FRET efficiency previously determined for ECFP in the same construct.[29] We then tested Aquamarine in a FRET biosensor of intracellular protein kinase A (PKA) activity. AMPc-dependent PKA is a central node in many intracellular signaling cascades that can be assayed by the AKAR biosensor and its multiple evolved versions.[2,3] AKAR is composed of a phosphoamino acid binding domain (FHA) and a PKA-specific substrate sandwiched between a cyan donor and a yellow acceptor. When phosphorylated by PKA, intramolecular binding of the substrate by the FHA domain drives a conformational reorganization, leading to an increase in FRET between the donor and the acceptor (Fig. 4A). AKAR2.2, composed of a CFP and a Citrine,[34] was modified into ^{Aq}AKAR^{Cit} by introducing the mutation T65S and H148G in the CFP donor. ^{Aq}AKAR^{Cit} was successfully expressed in BHK cells and its fluorescence was monitored on a microscopy setup equipped with a ratiometric FRET detection

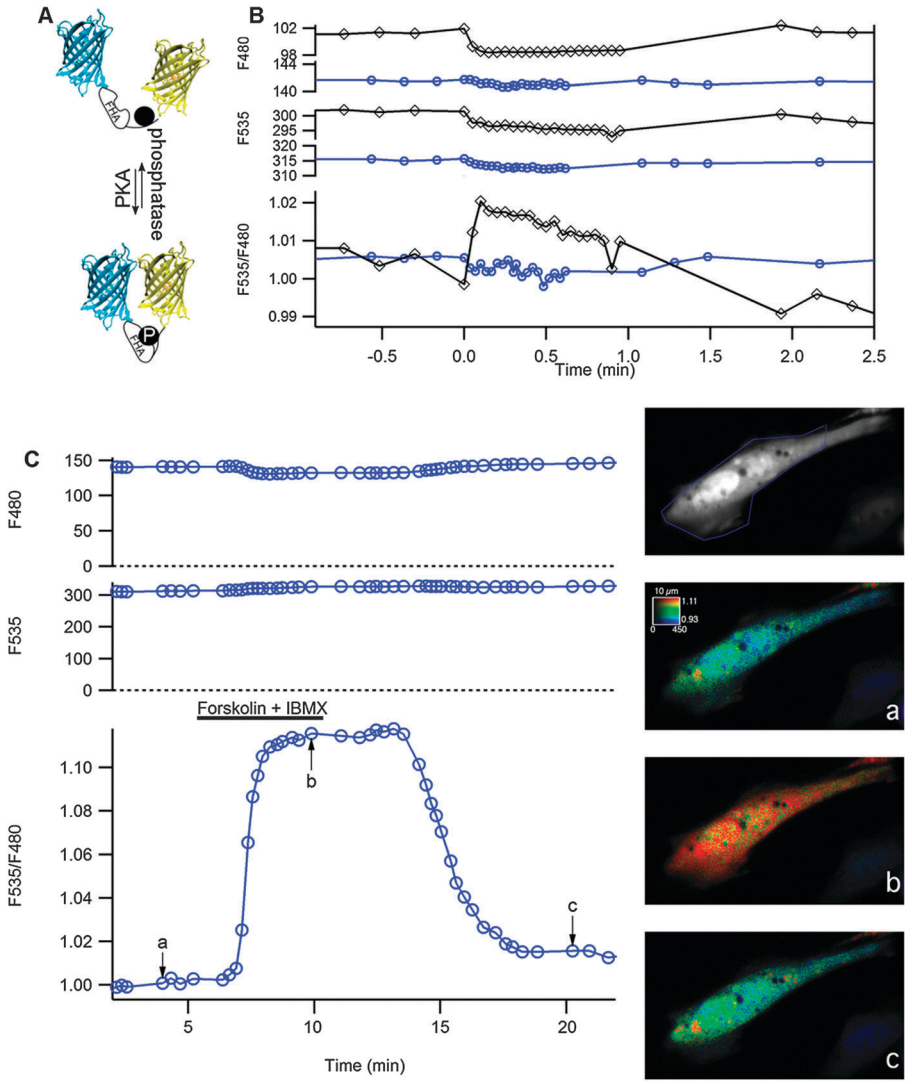

Fig. 4 ^{Aq}AKAR^{Cit} biosensor response in BHK cells. (A) Schematic representation of conformational reorganizations in AKAR upon phosphorylation by pK_a. (B) Absence of donor photoswitching in ^{Aq}AKAR^{Cit}: AKAR fluorescence intensities in the resting state upon a change in sampling frequency, in the case of Aquamarine (blue traces) or CFP (grey traces). Fluorescences at 480 nm, 535 nm and their ratio F535/F480 upon donor excitation at 436 nm. (C) Evolution of ^{Aq}AKAR^{Cit} fluorescence intensities upon activation of pK_a with 12.5 μM Forskolin, 100 μM of IBMX. On the right from top to bottom: intensity image of the cell and ROI used to calculate the average ratio plotted on the left, ratio images corresponding to points a, b and c on the F535/F480 trace.

(Fig. 4B and C). Using very low illumination levels, and in the absence of any activation, if the imaging frequency is increased while monitoring the basal fluorescence at 480 nm (monitoring direct CFP emission) and 530 nm (monitoring sensitized Citrine, plus some CFP fluorescence), a drop of AKAR2.2 fluorescence in both channels can be observed (Fig. 4B, black diamonds), a phenomenon that can be ascribed to the photoswitching of both CFP and Citrine: after one minute in the dark, the initial fluorescence is recovered. This perturbation leads to a significant increase, by a few percent, of the basal ratio trace (F530/F480). Upon the same treatment, the fluorescence of ^{Aq}AKAR^{Cit} is stable at 480 nm, whereas the signal at 530 nm dropped only slightly, resulting in a barely detectable variation of the basal ratio trace (Fig. 4B, blue circles).

We have measured the CFP fluorescence lifetimes in non-activated AKAR2.2, ^{Aq}AKAR^{Cit}, and in control variants where the absorbance of the Citrine acceptor has been suppressed by the Y66A mutation[29] (Fig. 3C). These controls show first that incorporation of ECFP into AKAR leads to some intrinsic perturbation of its fluorescence lifetime, as compared to the free cytosolic protein, while the lifetime of Aquamarine remains essentially insensitive to the fusion (Fig. 3C). Comparisons of average fluorescence lifetimes in the FRET constructs with Citrine show that the effective basal FRET before any activation is 19% in AKAR2.2, while it is 25% in ^{Aq}AKAR^{Cit}.

Then, we have studied the activation response of ^{Aq}AKAR^{Cit} in BHK cells incubated with forskolin and IBMX, respectively, activator of adenylyl cyclases and inhibitor of phosphodiesterases, expected to give rise to maximum AKAR responses.[35] The response of ^{Aq}AKAR^{Cit} is fast and reversible, with an average $\Delta R/R$ of 7–11% (Fig. 4C), quite comparable to the 10–12% response range of the original AKAR2.2 construct.

Controls incorporating the Y66A mutation indicate that about 2% of the activation response of AKAR2.2 result from direct perturbations of CFP fluorescence, while in the case of ^{Aq}AKAR^{Cit}, the amplitude response arises entirely from FRET changes.

Conclusion

We have shown that the simple combination of the T65S and H148G mutations is sufficient to achieve a prominent amelioration of ECFP, with near-optimum final performances similar to the best recently improved CFP forms. We also report on live cell imaging experiments that demonstrate the full ability of Aquamarine to work as a reliable FRET donor, together with its usual YFP partner. The transformation of ECFP-based fusion constructs towards their Aquamarine equivalents is a simple and easy method, relatively straightforward to implement with basic molecular biology facilities. As mTurquoise, Aquamarine will be well suited for quantitative FLIM analyses of FRET populations and binding equilibria, which require donors with single exponential emission decays.[30,36] Its brightness, its photostability and its much decreased environmental sensitivity will be beneficial also in dynamic FRET using ratiometric detection mode.

Similar mutations at positions 65 and/or 148 are found in all best improved CFP variants, and were successful in improving Cerulean or plasmids encoding CFPs with slightly different sequences. The fact that these two mutations can operate in different mutational contexts shows that their action on the CFP chromophore photophysics stems from quite general and robust mechanisms. We have already proposed a structural rationale for the improvements brought by the T65S mutation.[22] In the case of the H148G mutation, the fact that small aminoacids at position 148 resulted in the best performances suggests that a glycine simply gives the maximum space necessary to accommodate the bulky CFP chromophore. In this view, the multiple conformations of residue 148, observed in both ECFP[23,24] and Cerulean[37–39] would actually reflect the difficulty to incorporate large buried side chains at this position. Further, dedicated structural and dynamical studies will be necessary to substantiate this idea, and to understand the interplay between both mutations.

Materials and methods

Molecular biology procedures and protein sequence

ECFP refers to AvGFP F64L/S65T/Y66W/N146I/M153T/V163A/H231L (Clontech). Aquamarine (ECFP-65S, 148G), Aquamarine-72A, 206K (ECFP-65S, 72A, 148G, 206K) and mTurquoise (ECFP-65S, 72A, 148D, 175G, 206K) were obtained by multiple rounds of site-directed mutagenesis using the QuickChange Mutagenesis Kit from Stratagene on the ECFP variant in the plasmids described below. The mutation Y66A in the Citrine in AKAR was introduced with the same protocol. The list of oligonucleotides used for mutagenesis is shown in Table S1 (ESI†). For bacterial expression, ECFP was cloned in pProExHTa to produce a His-tagged protein (Invitrogen). For cytosolic expression pECFP-N1 (Clontech) was used. The pECFP-EYFP fusion contained ECFP and EYFP separated by a linker containing 27 amino acids. The previous plasmids were gifts of R. Grailhe, Institut Pasteur, Korea.[29] Connexin 43 sequence (a generous gift of C. Shao and D. Laird, University of Western Ontario, Canada)[27] was cloned in pECFP-N1 (Clontech) between KpnI and BamHI restriction sites. MyrPalm–CFP was obtained by genetically fusing an acylation substrate sequence from the 13 NH_2-terminal residues of the Lyn kinase to the N-terminus of CFP (generous gift from Tsien's lab[11]). The MyrPalm–CFP protein also carries the mutations K26R, N164H and L221K. The AKAR2.2 biosensor was a generous gift from J. Zhang (The Johns Hopkins University School of Medicine, Baltimore, USA).[34] The biosensor was cloned in pCDN3 and the CFP also carries the mutations K26R, N164H, A206K. All sequences were checked by DNA sequencing.

Purification and preparation of recombinant protein

Production and purification of His-tagged recombinant CFP variants was performed using TOP10 *E. coli* cells as described previously.[40] Bacterial growth, induction with isopropyl-β-D-thio-galactopyranoside, harvesting and lysis was performed as in ref. 40. Proteins were purified using a column loaded with Ni–NTA agarose beads (Sigma). The purified fusion protein His-CFP was further concentrated and the elution buffer was replaced either by a pH buffer (2 mM CAPS-MES-Bis–tris propane or 2 mM citric acid buffer, pH 7.4) or phosphate buffer 30 mM (pH 7.4) depending on their use. Protein concentration was quantified using a home-made Bicinchronic acid assay with BSA as the standard. Due to uncertainties in protein assays, all extinction coefficients reported in this study are within 10–15% error. SDS-PAGE of the purified protein shows a single band corresponding to 29 kD and sample purity was assessed to be superior to 95%.

Fluorescence spectroscopy

All spectroscopic measurements were performed at 20 °C as described in ref. 22. Buffer solutions contained 30 mM CAPS, 30 mM MES and 30 mM Bis–tris propane for pHs ranging from 11 to 5.5, and 50 mM citric acid for pHs ranging from 5.5 to 2.5. Aliquots from a concentrated protein solution in pH buffer were diluted into buffers previously adjusted to the appropriate pHs at 20 °C by addition of H_2SO_4 or NaOH. The final protein concentration was typically 10 μM for steady state and time resolved studies. Kinetic experiments of fluorescence recovery after denaturation and reduction were performed at 37 °C according to a protocol modified from ref. 41: Aquamarine and mTurquoise had to be heated for 15 min at 95 °C, in a denaturation buffer composed of 6.2 M GdmCl, 5 mM dithionite and 1 mM DTT, to achieve a significant level of denaturation and reduction, as assessed from changes in their absorption spectra. For consistency, ECFP was treated in the same way. During fluorescence recovery in the renaturation buffer, the reported time constants are those of the slowest phase, assumed to

correspond to the chromophore reoxidation step after fast protein refolding.[41]

Time resolved fluorescence spectroscopy. The fluorescence decays of purified CFPs were recorded at 20 °C using the time-correlated single photon counting technique (TCSPC) as described.[6,22] The excitation wavelength was 420 nm, the emission monochromator was set at 474 nm ($\Delta\lambda$ = 6 nm), and the instrumental response function (IRF) had a full-width at half maximum lower than 70 ps. Each experimental fluorescence decay curve $F(t)$ was analyzed individually together with its IRF using the maximum entropy method (MEM) as described in ref. 6 and 42.

This analysis assumes that the experimental decay $F(t)$ is the convolution product:

$$F(t) = g(t) \times \mathrm{Im}(t) \quad (1)$$

where $g(t)$ is a measured IRF, and $\mathrm{Im}(t)$ is the pure fluorescence decay law for instant excitation, described by a large number of decay times τ:

$$\mathrm{Im}(t) = I_0 \int_0^\infty a(\tau) \mathrm{e}^{-t/\tau} \mathrm{d}\tau \quad (2)$$

The fluorescence lifetime distribution $a(\tau)$ is thus the distribution of pre-exponential amplitudes, after normalization to unit zero-time intensity of the fluorescence decay law ($\int a(\tau)\mathrm{d}\tau$ = 1). The best model distribution $a(\tau)$ is recovered from the experimental decay without additional *a priori* assumptions, by simultaneously minimizing the reduced chi-square, while maximizing the entropy of the model.[42] For each protein, the lifetime distribution shown is an average of six independent experiments recorded at pH 7.4 and 20 °C. The average fluorescence lifetime τ_f is defined as the amplitude-averaged decay time:

$$\tau_f = \int_0^\infty a(\tau)\ \tau\ \mathrm{d}\tau \quad (3)$$

In the absence of any dark, absorbing but non-fluorescent population, this average lifetime bears a proportionality relationship to the fluorescence quantum yield.[6,42] The experimental errors on τ_f are the standard deviations over repeated identical experiments.

Fluorescence expression in *E. coli*

5 mL of a starter culture was grown overnight in LB supplemented with 100 μg mL^{-1} of ampicillin at 37 °C while shaking at 180 rpm. 50 mL of TB (supplemented with 100 μg mL^{-1} of ampicillin) was inoculated with 2 mL of the starter culture and grown to OD600 ~ 0.6. Cells were diluted to a OD600 = 0.1 and in a 96-well plate (Greiner) in the same growing medium containing also 0.5 mM IPTG (final volume, 200 μL). Their fluorescence (ex 440 nm, em 480 nm) and OD600 was monitored every 5 min by the microplate reader Synergy H1 equipped with monochromators (BioTek) during 20 h at 37 °C while shaking. For each protein, we averaged the fluorescence of 10 to 15 wells where bacterial growth were similar (monitored with the OD600) to that from two independent experiments. The fluorescence variation against time is presented as ±SD.

Live mammalian cell experiments

MDCK and BHK cell were cultivated in MEM GlutaMAX (Gibco) supplemented with 5% FCS in 25 cm^2 flasks. For microscopy, cells were grown on glass coverslip and transfected with Lipofectamine 2000 (Life technology) following the manufacturer's protocol. Cells were studied 24 to 48 hours after transfection.

For the experiments with AKAR, recordings were made on BHK cells grown on 10 mm Ø glass coverslips. Cells were activated with 12.5 μM of forskoline in the presence of phosphodiesterase inhibitor, IBMX, 100 μM. Lifetime, photostability and pH sensitivity of fluorescent proteins in live cells were performed in MDCK cells grown on 25 mm Ø glass coverslips. The intracellular pH was decreased by cell incubation in a buffer containing 15 mM of MES, 15 mM of Hepes and 140 mM of KCl at pH 5.9 in the presence of 10 μM nigericine.

Photoswitching and photobleaching experiments were performed at 20 °C under wide-field illumination at about 0.2 W cm^{-2} (field homogeneity better than 85%), as described in ref. 22. Transient and irreversible photobleaching kinetics were launched by sudden and constant illumination, after a prior, minimum 3 min dark equilibration of the sample. The illumination time was 15–20 s for photoswitching experiments and 30 min for photobleaching experiments. The fluorescence intensity was then checked for reversibility after 3 min in the dark. Reversibility after long term irradiation was less than a few percents. Each curve is an average of 4 to 6 decays collected from different cell individuals.

Cytometry

MDCK cells were transfected with equal amounts of DNA (4 μg). 24 h after transfection, cells were trypsinized, washed and resuspended in PBS and directly analyzed by flow cytometry with a CyFlowML cytometer (Partec) at room temperature. CFP fluorescence was excited at 405 nm and collected through a band pass filter (455/20 nm). Cells were gated and their fluorescence was analyzed to determine the percentage of fluorescent cells and their average fluorescence.

Confocal microscopy

Confocal images were recorded with a spinning disk confocal system (CXU-X1 A1, Yokogawa) mounted on an inverted microscope (Eclipse Ti, Nikon) equipped with a 100× oil immersion objective. Samples were excited at 405 nm and the fluorescence was detected at 447/60 nm on a EM-CCD (Evolve- 512 × 512 pix, Photometrics). The system was driven by Metamorph software.

Fluorescence lifetime imaging microscopy (FLIM)

Time-resolved laser scanning TCSPC microscopy was performed on a homemade setup based on a TE2000 microscope equipped with a 60×, 1.2NA water immersion objective (Nikon).

The pulsed excitation source was a LDH 440 pulsed diode laser driven by a PDL 800 driver (80 ps FWHM, 20 MHz of repetition rate, PicoQuant). The fiber coupled C1 scanning head (Nikon) was controlled by the EZ-C1 software (Nikon). The excitation beam crossed the epi-fluorescence filter turret, where neutral density filters were placed and was focused on the sample through the microscope's objective ($P < 1$ μW at sample). The scanning head probed a 100 × 100 μm maximum field of view with a laser pixel dwell time of 61.44 μs. The TCSPC detection was inserted in the collimated section just below the microscope objective. The pathway was composed of a cube containing a dichroic mirror positioned at 45° from the optical path (SWP-500, Lambda Research Optics), a focusing lens (f = 20 cm, Thorlabs), a set of filters to select the CFP fluorescence (480AF30, Omega) and reject the excitation light (two 458 nm Razor Edge Longpass, Semrock) and a detector (MCP-PMT, Hamamatsu). The signal was then amplified by a fast pulse preamplifier (Phillips Scientific) before reaching the PicoHarp 300 TCSPC module (PicoQuant). The counting rate of the recording was routinely between 50 000 and 100 000 cps. Lifetime measurements were analyzed by the PicoQuant SymPhoTime software (v5.3.2) which calculates the intensity image of the observed field of view. The TCSPC fluorescence decay of a chosen ROI was calculated by SymPhotTime and exported for further analysis in IGOR Pro (Wavemetrics). Each field of view was scanned enough times to accumulate 2–6 × 10^6 cts per decay. Mono, bi and tri exponential fits of the fluorescence decays were successively performed, and the average lifetime corresponding to the best residuals and the best chi square was kept for averaging. For each protein and each condition, averaged lifetimes for 10–20 cells were reported ±standard deviation. For the lifetime photostability assay, lifetime recordings with the FLIM setup alternate with bleaching steps performed with the epifluorescence light path.

Ratiometric FRET imaging

Wide-field images were obtained with an Olympus BX51WI upright microscope with a 40× 0.8 NA water-immersion objective and an ORCA-AG camera (Hamamatsu). Images were acquired with iVision (Biovision). The excitation and dichroic filters were D436/20 and 455dcxt. Signals were acquired by alternating the emission filters, HQ480/40 for CFP, and D535/40 for YFP, with a filter wheel (Sutter Instruments). All filters were obtained from Chroma Technology. Images were analyzed with custom routines written in the IGOR Pro environment (Wavemetrics). The emission ratio was calculated for each pixel. The pseudocolor images were calculated so as to display the ratio information (coded in hue) and the fluorescence of the preparation (coded in intensity) simultaneously. Only objective instrumental factors were corrected (camera offset and flat-field). No correction for bleed-through or direct excitation of the acceptor was applied.

Acknowledgements

AF acknowledges a doctoral grant from the French Ministry of Superior Education ad Research (MESR), and DBB a doctoral grant from the Centre de Compétences en Nanosciences, Région Ile-de-France (C'Nano IdF). PV acknowledges support from Ecole des Neurosciences Paris Ile-de-France. The TCSPC FLIM equipment was funded by a collaboration with Nikon France, a PPF from Université Paris-Sud and from ANR PCV-2007. This work has benefited from the facilities and expertise of the Imagif Cell Biology Unit of the Gif campus (www.imagif.cnrs.fr) which is supported by the Conseil Général de l'Essonne. We wish to thank in particular M. N. Soler for her help in data acquisition. Cytometry data were recorded on the cytometer of the INSERM UMR-S757 Unit with the kind help of O. Nüsse.

References

1 E. Kiyokawa, K. Aoki, T. Nakamura and M. Matsuda, *Annu. Rev. Pharmacol. Toxicol.*, 2011, **51**, 337–358.
2 X. Zhou, K. J. Herbst-Robinson and J. Zhang, *Methods Enzymol.*, 2012, **504**, 317–340.
3 P. Vincent, N. Gervasi and J. Zhang, *Brain Cell Biol.*, 2008, **36**, 3–17.
4 M. Tramier, M. Zahid, J. C. Mevel, M. J. Masse and M. Coppey-Moisan, *Microsc. Res. Tech.*, 2006, **69**, 933–939.
5 N. C. Shaner, M. Z. Lin, M. R. McKeown, P. A. Steinbach, K. L. Hazelwood, M. W. Davidson and R. Y. Tsien, *Nat. Methods*, 2008, **5**, 545–551.
6 A. Villoing, M. Ridhoir, B. Cinquin, M. Erard, L. Alvarez, G. Vallverdu, P. Pernot, R. Grailhe, F. Merola and H. Pasquier, *Biochemistry*, 2008, **47**, 12483–12492.
7 J. W. Borst, M. Willemse, R. Slijkhuis, G. van der Krogt, S. P. Laptenok, K. Jalink, B. Wieringa and J. A. Fransen, *PLoS One*, 2010, **5**, e13862.
8 J. Goedhart, L. van Weeren, M. A. Hink, N. O. Vischer, K. Jalink and T. W. Gadella Jr., *Nat. Methods*, 2010, **7**, 137–139.
9 M. L. Markwardt, G. J. Kremers, C. A. Kraft, K. Ray, P. J. Cranfill, K. A. Wilson, R. N. Day, R. M. Wachter, M. W. Davidson and M. A. Rizzo, *PLoS One*, 2011, **6**, e17896.
10 J. Goedhart, D. von Stetten, M. Noirclerc-Savoye, M. Lelimousin, L. Joosen, M. A. Hink, L. van Weeren, T. W. Gadella Jr. and A. Royant, *Nat. Commun.*, 2012, **3**, 751.
11 D. A. Zacharias, J. D. Violin, A. C. Newton and R. Y. Tsien, *Science*, 2002, **296**, 913–916.
12 D. von Stetten, M. Noirclerc-Savoye, J. Goedhart, T. W. J. Gadella and A. Royant, *Acta Crystallogr., Sect. F: Struct. Biol. Cryst. Commun.*, 2012, **68**, 878–882.
13 A. Espagne, M. Erard, K. Madiona, V. Derrien, G. Jonasson, B. Levy, H. Pasquier, R. Melki and F. Merola, *Biochemistry*, 2011, **50**, 437–439.
14 B. P. Cormack, R. H. Valdivia and S. Falkow, *Gene*, 1996, **173**, 33–38.
15 G. H. Patterson, R. N. Day and D. W. Piston, *J. Cell Sci.*, 2001, **114**, 837–838.
16 G. J. Kremers, J. Goedhart, D. J. van den Heuvel, H. C. Gerritsen and T. W. J. Gadella, *Biochemistry*, 2007, **46**, 3775–3783.
17 G. J. Kremers, J. Goedhart, E. B. van Munster and T. W. J. Gadella, *Biochemistry*, 2006, **45**, 6570–6580.
18 R. Heim, A. B. Cubitt and R. Y. Tsien, *Nature*, 1995, **373**, 663–664.
19 M. A. Rizzo, G. H. Springer, B. Granada and D. W. Piston, *Nat. Biotechnol.*, 2004, **29**, 445–449.
20 X. Shu, K. Kallio, X. Shi, P. Abbyad, P. Kanchanawong, W. Childs, S. G. Boxer and S. J. Remington, *Biochemistry*, 2007, **46**, 12005–12013.
21 A. Esposito, M. Gralle, M. A. Dani, D. Lange and F. S. Wouters, *Biochemistry*, 2008, **47**, 13115–13126.
22 A. Fredj, H. Pasquier, I. Demachy, G. Jonasson, B. Levy, V. Derrien, Y. Bousmah, G. Manoussaris, F. Wien, J. Ridard, M. Erard and F. Merola, *PLoS One*, 2012, **7**, e49149.
23 J. H. Bae, M. Rubini, G. Jung, G. Wiegand, M. H. J. Seifert, M. K. Azim, J. S. Kim, A. Zumbusch, T. A. Holak, L. Moroder, R. Huber and N. Budisa, *J. Mol. Biol.*, 2003, **328**, 1071–1081.
24 M. H. Seifert, D. Ksiazek, M. K. Azim, P. Smialowski, N. Budisa and T. A. Holak, *J. Am. Chem. Soc.*, 2002, **124**, 7932–7942.

25 H. C. Chang, C. M. Kaiser, F. U. Hartl and J. M. Barral, *J. Mol. Biol.*, 2005, **353**, 397–409.
26 D. M. Chudakov, M. V. Matz, S. Lukyanov and K. A. Lukyanov, *Physiol. Rev.*, 2010, **90**, 1103–1163.
27 K. Jordan, J. L. Solan, M. Dominguez, M. Sia, A. Hand, P. D. Lampe and D. W. Laird, *Mol. Biol. Cell*, 1999, **10**, 2033–2050.
28 M. D. Resh, *Biochim. Biophys. Acta, Mol. Cell. Res.*, 1999, **1451**, 1–16.
29 R. Grailhe, F. Merola, J. Ridard, S. Couvignou, C. Le Poupon, J. P. Changeux and H. Laguitton-Pasquier, *ChemPhysChem*, 2006, **7**, 1442–1454.
30 K. A. Walther, B. Papke, M. B. Sinn, K. Michel and A. Kinkhabwala, *Mol. BioSyst.*, 2011, **7**, 322–336.
31 J. W. Borst, M. A. Hink, A. van Hoek and A. J. W. G. Visser, *J. Fluoresc.*, 2005, **15**, 153–160.
32 B. Young, R. Wightman, R. Blanvillain, S. B. Purcel and P. Gallois, *Plant Methods*, 2010, **6**, 27.
33 D. Sinnecker, P. Voigt, N. Hellwig and M. Schaefer, *Biochemistry*, 2005, **44**, 7085–7094.
34 T. A. Dunn, C. T. Wang, M. A. Colicos, M. Zaccolo, L. M. DiPilato, J. Zhang, R. Y. Tsien and M. B. Feller, *J. Neurosci.*, 2006, **26**, 12807–12815.
35 L. R. V. Castro, N. Gervasi, E. Guiot, L. Cavellini, V. O. Nikolaev, D. Paupardin-Tritsch and P. Vincent, *J. Neurosci.*, 2010, **30**, 6143–6151.
36 F. Cardarelli, R. Bizzarri, M. Serresi, L. Albertazzi and F. Beltram, *J. Biol. Chem.*, 2009, **284**, 36638–36646.
37 G. D. Malo, L. J. Pouwels, M. Wang, A. Weichsel, W. R. Montfort, M. A. Rizzo, D. W. Piston and R. M. Wachter, *Biochemistry*, 2007, **46**, 9865–9873.
38 M. Lelimousin, M. Noirclerc-Savoye, C. Lazareno-Saez, B. Paetzold, S. Le Vot, R. Chazal, P. Macheboeuf, M. J. Field, D. Bourgeois and A. Royant, *Biochemistry*, 2009, **48**, 10038–10046.
39 G. Vallverdu, I. Demachy, F. Merola, H. Pasquier, J. Ridard and B. Levy, *Proteins*, 2010, **78**, 1040–1054.
40 L. Alvarez, C. Houee-Levin, F. Merola, T. Bizouarn, H. Pasquier, L. Baciou, F. Rusconi and M. Erard, *Photochem. Photobiol.*, 2010, **86**, 55–61.
41 T. Nagai, K. Ibata, E. S. Park, M. Kubota, K. Mikoshiba and A. Miyawaki, *Nat. Biotechnol.*, 2002, **20**, 87–90.
42 F. Merola, R. Rigler, A. Holmgren and J. C. Brochon, *Biochemistry*, 1989, **28**, 3383–3398.